METHODOLOGY DEVELOPMENT FOR SULPHUR DETECTION IN OIL SHALE USING X-RAY FLUORESCENCE SPECTROMETRY

Master thesis

Student
Erki Leht
212093
Supervisor
Alar Konist
Professor
Co-Supervisor
Jaan Kalda
Professor

Tallinn 2024

Declaration

Hereby I declare that I have compiled the paper independently and all works, important standpoints and data by other authors have been properly referenced and the same paper has not been previously been presented for grading.

Author: Erki Leht
Signed digitally, 02.01.2023

The paper conforms to requirements in force.
Supervisor: Alar Konist
Signed digitally, 02.01.2023

Co-supervisor: Jaan Kalda
Signed digitally, 02.01.2023

Permitted to the defence.
Chairman of the defence: name
signature and date

Table of contents

Introduction **5**

1 Theory **6**

1.1 Overview of X-ray fluorescence spectrometry 6
1.2 X-rays 6
1.3 Scattering 7
1.3.1 Compton Scattering 7
1.3.2 Rayleigh scattering 8
1.4 Absorption and fluorescence 9
1.4.1 Absorption 9
1.4.2 Fluorescence 10
1.5 Spectra 11
1.5.1 Common notation of spectral lines 11
1.5.2 Continuous spectra 11
1.5.3 Characteristic spectra 12
1.6 X-ray sources 13
1.7 Wavelength Dispersive X-Ray Fluorescence 15
1.8 Sulphur and oil shale 16
1.9 Fluorescence yield and the Auger effect 17
1.10 Uncertainty 17

2 Methodology development for sulphur detection in oil shale using X-ray fluorescence spectrometry **18**

2.1 Main devices 18
2.2 Development process 19
2.3 Preparation of samples 19
2.3.1 Basic principle 19
2.3.2 Solid 20
2.3.3 Powder 20
2.3.4 Press pellet 20
2.3.5 Beads 22
2.3.6 Liquid 23
2.4 Sample reagents 23
2.5 Optimization 24
2.6 Quantitative analysis 24
2.6.1 Results, pressed pellets 24
2.6.2 Results, beads 27
2.6.3 Pressed pellets versus fused beads 29

3 Summary **31**

4 Acknowledgements **32**

5 Reference material **33**

Abstract

The purpose of this thesis was to determine the optimal conditions for analysis of sulphur in X-ray fluorescence spectrometers. For this purpose, multiple samples of oil shale ash were analysed both in the form of pressed pellets of two sizes and fused glass beads. Characteristics of special interest were the amount of energy and time expended to achieve satisfactory results.

Additionally, statistical analysis of repeated XRF sample testing was examined. This was achieved by firstly testing sets of samples multiple times in identical conditions and within the same X-ray fluorescence analyser, then the results were investigated. This investigation included outlining the results through graphs and determining the type-A uncertainty for both pellet and bead samples.

The shale oil ash used for the samples were gathered from the Auvere power plant in Ida-Virumaa. They were analysed using two wavelength dispersive X-ray fluorescence devices which utilise different methods for sequential analysis. The results were tabulated and analysed.

The gathered information indicates that even sub-optimal conditions can return relatively reliable data on the sulphur content of oil shale. On average, fused beads have lower sulphur levels than pressed pellets, and pressed pellets may also experience sulphur content variance due to a difference in binding materials or size. The divergence between testing results of different machines is minimal, the deviations of testing sets is explainable by measurement uncertainty.

Introduction

Estonia has one of the most developed oil shale industries in the world (International Energy Agency, 2013), thus its proper usage and mitigation of pollution remains a pertinent topic. Of the polluting elements, one of the most important is sulphur, as its oxides are harmful to plant life and potentially even animal and human health. To prevent the introduction of excess sulphur into the environment, it is first necessary to develop expedient ways of detecting its concentration within the fuel and its remains following combustion. One ideal candidate for detection is a non-destructive method called X-ray fluorescence spectrometry. While this method is a popular and reliable one, it has by no means been perfected; there are plenty of opportunities to improve the time and energy efficiency.

For this purpose, a more in-depth analysis of different sample preparation methods and the benefits of each would be prudent to determine which ones would be optimal for repeated measuring of sulphur from oil shale. Additionally, a difference in utilized devices and repeated testing could affect the resulting information. Clarifying both of these issues constitutes the purpose of this thesis.

This thesis consists of two parts:

- the first is an overview of the fundamental theory behind X-ray fluorescence, the physics behind it and the construction of devices that measure concentrations of chemical elements using X-ray fluorescence,
- the second is a description of the sample creation and analysis methods utilized, as well as an examination of the data acquired from the tests.

The topic of the thesis was chosen due to an interest in X-ray fluorescence spectrometry and a desire to improve the methods and knowledge involved in analysis of fuels, particularly oil shale.

1 Theory

1.1 Overview of X-ray fluorescence spectrometry

X-ray fluorescence (henceforth referred to as "XRF") spectrometry is a non-destructive analytical method of determining the chemical composition of multiple types of materials. While the analysed material is not restricted into certain states, they are mainly solid, liquid or powder. Analysable materials range from minerals and soil samples to industrial products such as ceramics or petroleum. Specifically, XRF systems can clearly differentiate elements from sodium to uranium, with higher atomic number elements having better detection limits than lighter elements. (Brouwer, 2013)

XRF systems can be divided into two main groups:

- Energy dispersive systems (EDXRF), which sort output X-rays depending on their energy.
- Wavelength dispersive systems (WDXRF), which sort output X-rays depending on their wavelength. Have a wider range of elements that it can differentiate, from beryllium to uranium. (Brouwer, 2013)

Given identical samples, the results of the two systems are very similar, mean values are coincident within one standard deviation of all elements (Tugulan et al, 2016). The preferred type of system is entirely dependent on the nature of the samples and the research being conducted.

1.2 X-rays

X-rays are a form of electromagnetic radiation. They have relatively high energies, ranging from 0.1 to 100 keV, with a corresponding wavelength range of 10 to 0.01 nm (Murphy et al., 2017), placing them between ultraviolet radiation and gamma rays. They can be interpreted as either waves or beams of photons, both of which have an associated measurable property: wavelength for waves and energy for photons. These two properties are inversely proportional to each other, this can be expressed using the Planck-Einstein relation:

$$E = h \cdot f = h \cdot \frac{c}{\lambda} \tag{1}$$

where E is the energy of the photon, λ is the wavelength of the electromagnetic wave, c is the speed of light in a vacuum, and h is the Planck constant with a value of $h = 1.240keV \cdot ns$, assuming the units for energy and wavelength are keV and nm. (Brouwer, 2013)

X-rays are undetectable by human senses, but can be detected by physical instruments through X-ray's interactions with matter, which include transmission, reflection, diffraction and photoelectric absorption, the last of which includes the photoelectric effect (Willis and Duncan, 2008). The type of interaction that occurs when the radiation encounters the sample

is dependent on the nature of the sample and the energy of the photon, barring any random results due to quantum indeterminacy (Fewster, 2015). Of these interactions, absorption is the most pertinent to XRF spectrometry, as it causes the spectra from which information about analysed material can be derived.

There are two types of spectra that are relevant in XRF spectroscopy:

- *Brehmsstrahlung*, is a type of dipole radiation that is caused by the acceleration of electrons, though in terms of physics, it can be handled as cyclotron radiation. It is detected as a continuous spectrum.
- Characteristic line spectra consist of a series of discrete wavelengths, which are characteristic of the element from which they were emitted. The wavelengths have fixed relative intensities for a given element. (Willis and Duncan, 2008)

1.3 Scattering

X-ray scattering is a physical process in which the path of an X-ray is forced to deviate due to interaction with a particle. In the field of XRF spectrometry, this medium is the sample being analysed. As X-ray photons are electromagnetic radiation, they interact with both electric and magnetic field, though the electric field vector has undeniably the stronger of the two interactions with the sample. Magnetic interaction is negligible and becomes observable under special circumstances with a very intense source of X-rays. (Fewster, 2015)

Scattering relevant to XRF spectroscopy can be divided into Compton scattering and Rayleigh scattering. While both types of scattering contribute to the modification of the primary XRF line (Fernandez, 1992), they are ultimately not a source of information about the sample itself.

1.3.1 Compton Scattering

Compton scattering is the interaction of a photon with a free electron. The photon loses part of its energy through elastic collision with one of the electrons of a material that it passes through (Turchetta, 2014). As the photon collides with an electron that is loosely bound to an atom, such as a valence electron, a portion of the photons energy is transferred to the electron, ejecting it from the atom's orbit. As the energy of the photon lowers, its direction is changed compared to the original trajectory (Figure 1).

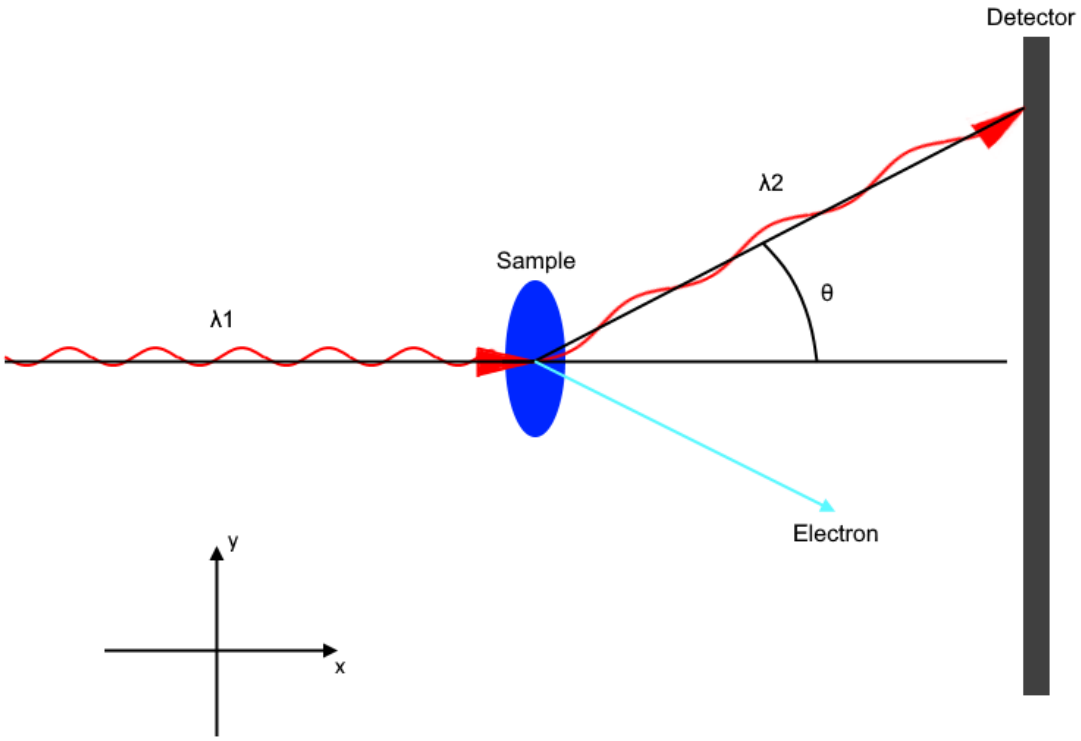

Figure 1. Compton scattering of a single photon.

According to equation (1), a change in energy of a photon must correspond to a change in wavelength. This change in wavelength can be related to the scattering angle:

$$\Delta\lambda = \lambda_2 - \lambda_1 = \frac{h}{mc} \cdot (1 - \cos 2\theta) \tag{2}$$

where λ_1 and λ_2 are respectively the wavelengths of the incident and scattered photons, h is Planck's constant, m is the electron's rest mass, c is the velocity of light in a vacuum and θ is the change in the direction of the photon's trajectory. (Hamouda, 2020)

The ratio $\frac{h}{mc} = 2.426 \times 10^{-12}\,\text{m}$ is referred to as the *Compton wavelength*, as it has corresponds to the rest energy of an electron, 0.51 MeV, and therefore results in more noticeable occurrences of the Compton effect (Hamouda, 2020).

1.3.2 Rayleigh scattering

Rayleigh scattering is similar to Compton scattering in that it results in the change in direction for electromagnetic radiation. Unlike Compton scattering, Rayleigh scattering does not require the photon to encounter a charged particle, only the size of the particle relative to the wavelength of the electromagnetic radiation is relevant. Namely, the size of the particle

must be much smaller than the wavelength of the incident radiation (Rojo and Berman, 2010).

The most important distinction from Compton scattering is that Rayleigh scattering does not result in a change of energy for the photon, only a change in direction (Fernandez, 1992). This also means that Rayleigh scattering is a parametric process, meaning it does not change the quantum state of the materials it occurs upon.

1.4 Absorption and fluorescence

The primary source of continuous and characteristic line spectra is the phenomenon of absorption and the fluorescence that occurs with it, as can be seen in the name of the particular spectrometry method used in this thesis, XRF — X-ray **fluorescence**.

1.4.1 Absorption

Absorption is a process in which matter converts the energy of a photon that has interacted with it into internal energy, such as heat (Baird, 2019). Absorption occurs when X-rays interact with strongly bound electrons near the nucleus of the atom. For X-ray photons of sufficient energy, photoelectric absorption is most likely to be caused by electrons with stronger binds to the nucleus, as the concentration of these electrons is highest (Hussein, 2007).

When an incident photon reaches a strongly bound electron, the subsequent behaviour of the charged particle is dependent on the difference between the energy of the photon and the binding energy of the particle. If the binding energy of the electron is greater than the energy of the photon, the electron will not be perturbed and the photon is not absorbed. If the binding energy of the electron is lower than the energy of the photon, the electron can be removed from the atom, with all excess energy of the photon converted into kinetic energy for the newly ejected photoelectron. This phenomenon is also referred to as the photoelectric effect. (The Photoelectric Effect, 2016)

The kinetic energy of the photoelectron is calculable through the equation:

$$E_k = E_{photon} - \phi = h \cdot f - \phi \tag{3}$$

where E_k is the kinetic energy of the photoelectron, ϕ is the binding energy of the electron, E_{photon} and f are the energy and frequency of the photon, respectively, and h is Planck's constant. (Schäfers et al, 2014)

Notably missing from equation (3) is the intensity of the radiation. It can be assumed then, that intensity is not a factor in the final kinetic energy of a given photoelectron, but it does influence the amount of electrons displaced in total.

1.4.2 Fluorescence

In order to aid in understanding the process of fluorescence, the Bohr model of the atom is used, i.e. it is assumed that electrons inhabit different "orbits" around the nucleus, with electrons on closer orbits being more strongly bound to the nucleus than those further away. The departure of the photoelectron leaves a gap in the electron shell, one that is nearly immediately filled by electrons from higher energy levels. To relocate to these lower levels, the electrons on the higher levels must relinquish a portion of their own internal energy. This is done by emission of photons with energies equal to the difference of energies between the higher level orbit the relocating currently inhabits and the lower level orbit of the electron vacancy. As can be observed on figure (2), this creates a chain reaction of photon emissions, as each electron relocating to fill in a vacancy creates a new vacancy that an even higher electron will reposition to. This process is very fast, taking place within 10^{-12} to 10^{-14} seconds when an electron vacancy is created. (Willis and Duncan, 2008)

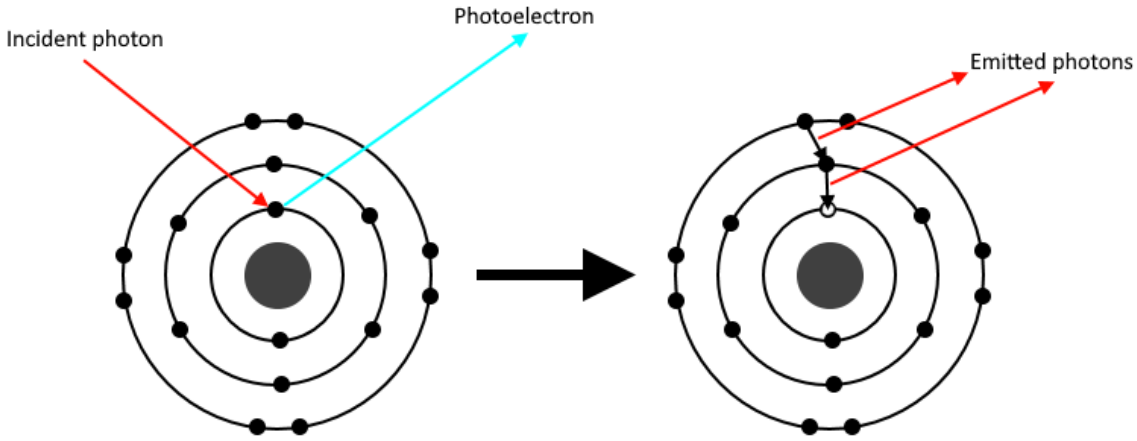

Figure 2. Schematic diagram showing a chain reaction triggered by the loss of a photoelectron and contributing to the X-ray fluorescence.

It must be noted that photons are not the sole method of inducing excitations, free electrons with sufficient speed may also interact and give a part of their kinetic energy to strongly bound electron, ejecting it from orbit and causing an identical process of electron relocation and photon emission to begin. (Kang and Foland, 1967)

The difference of energies is characteristic for every chemical element independent of their environment, thus making fluorescence a feasible non-destructive source of information about the chemical composition of a given sample (Etim and Rebecca, 2022). This forms the basis of XRF spectrometry, the acquisition and analysis of XRF spectra.

The limitations of XRF spectrometry are due to the nature of fluorescence. Firstly, fluorescence can only affect individual atoms, the bonds between atoms do not affect the outcome

of XRF spectrometry. Thus, the elements that the molecule contains can be detected, but no information on how the molecule itself is constructed. Secondly, lighter elements require high resolutions, as the photons released from fluorescence are low in energy. These low energy photons have a high probability of being absorbed by elements within the medium in which the XRF procedure is carried out. (Brouwer, 2013)

1.5 Spectra

X-ray spectra are similar to optical emission spectra, but are far less complex, as they have fewer spectral lines due to originating from electron transitions from inner orbitals. The inner orbitals have fewer electrons than the outer orbitals that are involved in optical emission spectra, therefore producing far fewer lines. (Willis and Duncan, 2008)

1.5.1 Common notation of spectral lines

As X-ray spectra are the result of the movement of electrons between different levels of the electron shell surrounding the nucleus, it would be prudent to use atomic orbital notation to simplify the spectra creation process. In fact, X-ray science has a specialized form of notation specifically to describe the transition of electrons from upper to lower energy levels. The standard used today is the IUPAC (International Union of Pure and Applied Chemistry) notation, which itself is a refinement of the Siegbahn notation. However, much of XRF terminology is named after the older Siegbahn notation, and IUPAC notation in general has not seen widespread use, meaning knowledge of Siegbahn notation is sufficient to understand XRF. (Jenkins et al, 1991)

The Siegbahn notation for a X-ray consists of 2 parts, a letter of the Latin alphabet and a letter from the Greek alphabet with an index: A_{μ_j}, where A indicates the energy level the electron has shifted to, using letters from the Latin alphabet starting from K in decreasing order of energy. μ denotes the starting energy level of the relocated electron, with α indicating relocation from one level above the A energy level, β from two levels and so on. Accordingly, μ follows a descending order of intensity, with α being the most intense, β being less intense and so on. As these X-rays actually occur in groups, the index number j is used to differentiate between the different lines, with the index missing entirely if the entire group of rays is referred to as a whole. j is also in a descending order of intensity: 1 is the most intense, 2 is less intense, etc. (Jenkins et al, 1991)

1.5.2 Continuous spectra

The source of continuous spectra is *bremsstrahlung* or "braking" radiation, which in turn is caused by fluorescence photoelectrons reaching a target anode. Specifically, the high-speed photoelectron interacts with the nuclei of matter, experiencing gradual deceleration, reducing its kinetic energy as photons which are registered by the detector. The output from the detector is a wide spectrum of photon wavelengths or energies, which is caused by the abundance

of different interactions a charged particle may have inside matter. (L'Annunziata, 2003)

In practical terms, continuous spectra are not characteristic to different chemical elements, meaning they can be considered to be "background information". They do not give decisive information about the chemical composition of the sample.

The intensity of the continuous spectrum is zero until a certain wavelength referred to as the short wavelength limit. After the limit, the intensity grows until it reaches a maximum, after which it begins to decrease. There is no hard limit for how long of a wavelength there may be in a continuous spectrum. The appearance of the continuous spectrum when plotted on an intensity versus wavelength graph is approximated by Kramer's law: (Laguitton and Parrish, 1977)

$$I(\lambda)\mathrm{d}\lambda = K\left(\frac{\lambda}{\lambda_{\min}} - 1\right)\frac{d\lambda}{\lambda^2} \tag{4}$$

where λ is wavelength of emitted X-rays, I is the intensity of the radiation, and K is a constant that is proportional to the atomic number of the element. (Laguitton and Parrish, 1977)

1.5.3 Characteristic spectra

Characteristic spectra are caused by photons emitted through fluorescence. These photons transfer all of their energy as they reach the detector (Willis and Duncan, 2008). This energy is unique to the chemical element that it was emitted by, as previously established. As X-rays that are caused by electrons moving to the same energy level have similar wavelengths, they are commonly grouped accordingly, with groups being named after the electron shell from where they were removed. For example, characteristic lines that are caused by electrons transitioning to a K-shell orbit are called "K series lines". (Guthrie and Ferguson, 2012)

Characteristic lines have the appearance of sharp, sudden spikes when plotted on an intensity versus wavelength graph. Combining characteristic lines with the continuous spectra gives a final spectrum for XRF analysis (figure 3).

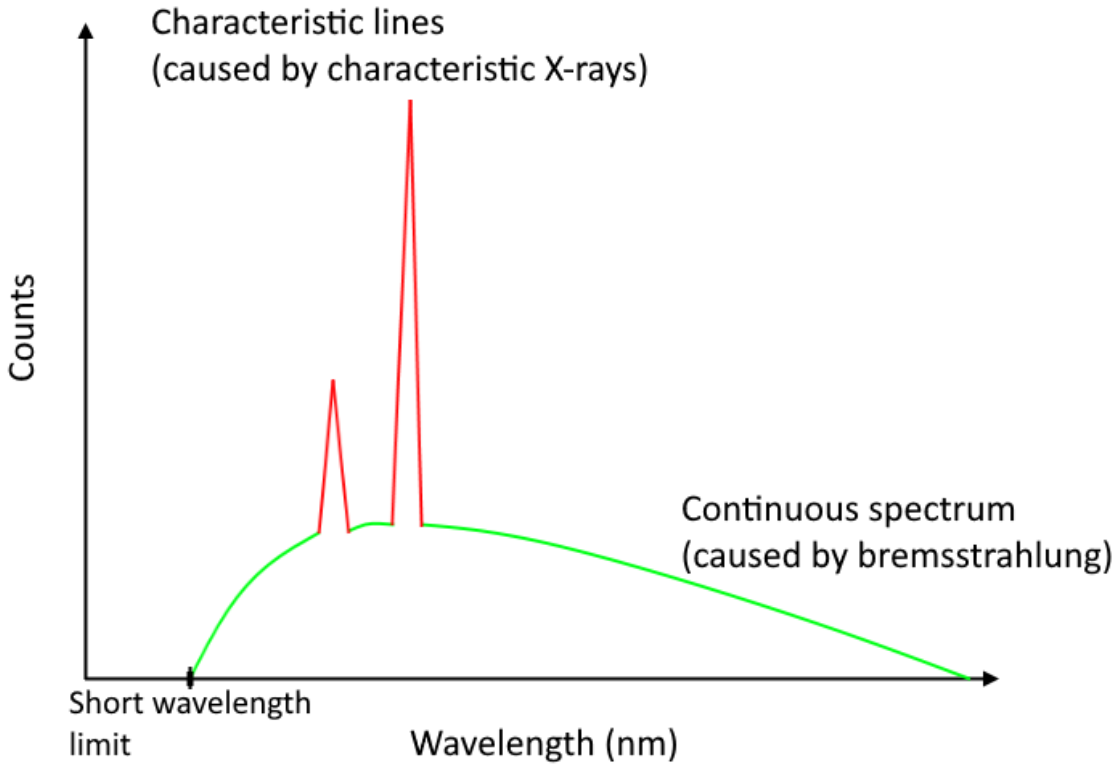

Figure 3. Simplified example of a final spectrum, X-ray outputs sorted by wavelength.

As inner electron orbitals are not affected by the valence state of the atom, the X-ray line wavelength and the atomic number of the excited element are relative to each other (Willis and Duncan, 2008). This was mathematically expressed by Henry Moseley in 1913, in the form of Moseley's Law:

$$\lambda \propto \frac{1}{Z^2} \tag{5}$$

where λ is the wavelength of the characteristic X-ray line and Z is the atomic number of the element (Darwell, 2018). As there is an inverted square relation between the atomic number of an element and the wavelength of its characteristic X-ray lines, according to equation (1), there must also be a square relation between the atomic number and the energy of the characteristic lines.

1.6 X-ray sources

Without a reliable source of X-rays, the idea of XRF analysis would be purely theoretical. Thus, any machine that would facilitate XRF analysis must contain a source of high energy X-rays, which they do in the form of X-ray tubes. An X-ray tube is a vacuum tube that generates X-ray radiation when an energetic beam of electrons meets an anode, which are made of metal, usually tungsten, copper or molybdenum. Excitation of characteristic X-rays within the sample can be optimized by selecting the appropriate anode material, voltage and tube current. (Kramar, 1999)

A common problem with X-ray tubes is the heat generated by the stream of electrons encountering matter, which naturally limits the power at which the device can be operated and thereby the intensity of the resulting X-ray beam. There exist multiple solutions for this, such as water cooling, rotating the anode to prevent overheating or focusing the electron beam to a smaller point, but overheating remains the principal limiting factor for X-ray beam intensity. (Gonzalez, 2012)

The heat buildup within the anode is measured with heat units, which are defined as $HU = kVp \cdot mA \cdot s$, where HU is heat units, kVp is peak kilovoltage (the maximum potential applied to the X-ray tube), mA is milliamperes, and s is seconds (White and Pharoah, 2014).

X-ray vacuum tubes generally consist of a cathode filament, a cathode cap to catch stray electrons, a focusing tube to focus electrons into a beam before they reach the anode, and the anode itself, which usually has a water-cooling element to prevent overheating (figure 4).

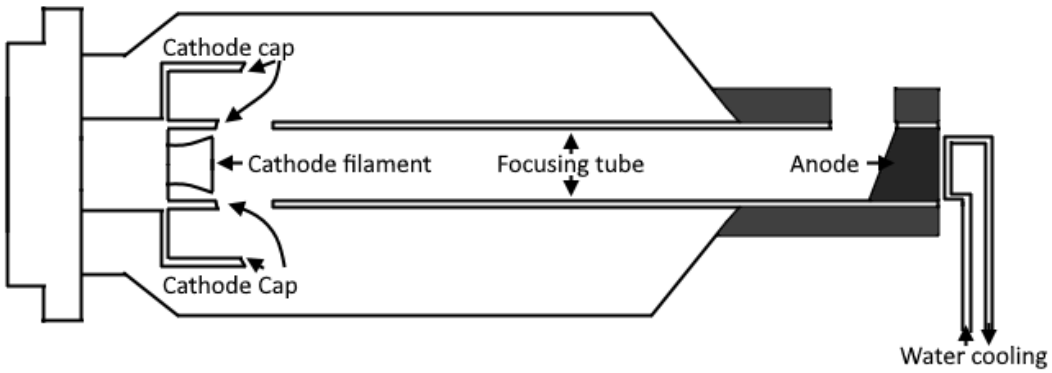

Figure 4. Simplified construction of an X-ray tube.

The excitation of electrons requires high-energy photons, which logically means that there must be a minimum required energy to induce fluorescence. This energy is more properly defined as excitation potential, which is the minimum energy required in volts by an electron or photon in order to remove a specified electron from the orbital of an atom. In XRF device terms, the excitation is the minimum potential that the X-ray source must operate at to produce the characteristic lines of a sample. There exist multiple excitation potentials for every element, specifically, there is one for every electron orbital, as can be seeon on table 1. (Willis and Duncan, 2008)

Element	K	L_{III}	M_V
Sc	4.5	0.41	-
Cr	6.0	0.57	-
Mo	20.0	2.52	0.23
Rh	23.2	3.00	0.32
W	69.5	10.2	1.80
Au	80.7	11.9	2.22

Table 1. Excitation potentials in kilovolts for common X-ray tube target elements. K, L_{III} and M_V are notation for K-level orbital, the third sublevel of a L-level orbital and the fifth sublevel of a M-level orbital, respectively.

1.7 Wavelength Dispersive X-Ray Fluorescence

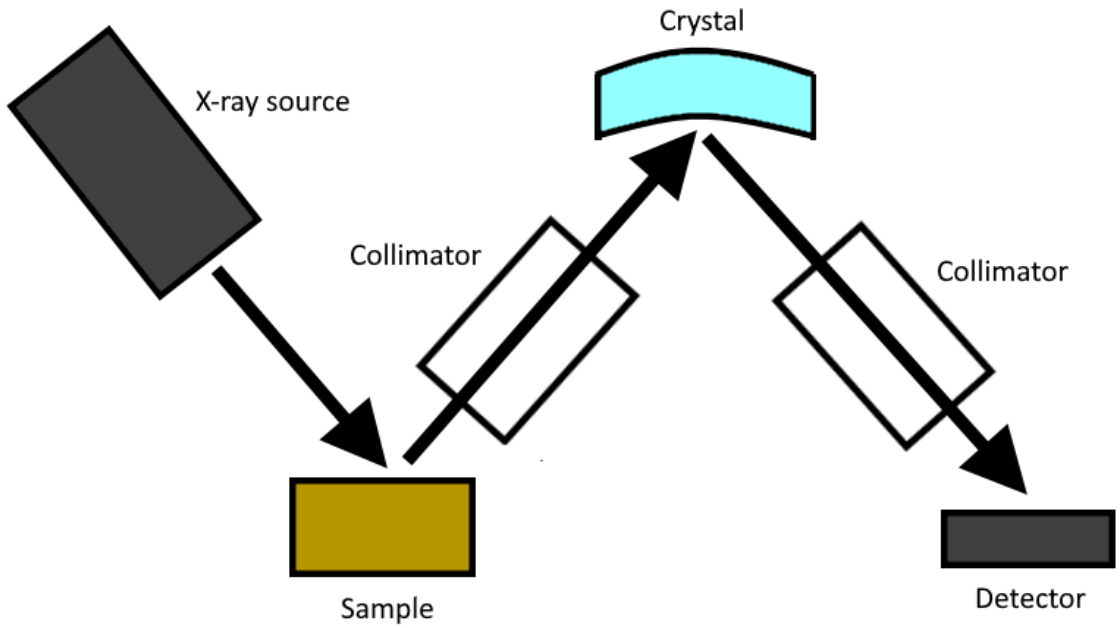

Figure 5. Simplified construction of a WDXRF.

WDXRF uses elements known as crystals to disperse the spectrum caused by fluorescence into individual wavelengths. The crystals may be made of minerals, metallic, synthetic or organic layers, with different materials affecting the sensitivity and resolution of the machine in addition to the temperature and X-ray resistance of the crystals themselves. (Brouwer, 2013)

The crystals represent the basis for the functionality of WDXRF machines, Bragg's law, which states that an incident X-ray meeting a crystal surface will reflect with the same angle with which it arrived, with reflections only occurring with specific wavelengths and incident angles causing constructive interference between different X-rays. This law can be given in the form: (Kramar, 1999)

$$n \cdot \lambda = 2 \cdot d \cdot \sin\theta \quad (6)$$

Where n is an integer, λ is the wavelength of the incident X-ray, d is the space between layers of crystal and θ is the incident and reflective angle of the X-ray. (Kramar, 1999)

From Bragg's law it can be assumed that the angles of the crystals or the detector can be changed in order to regulate what wavelengths are able to be measured with a WDXRF machine. However, the use of crystals to measure wavelengths presents a different problem: X-rays may reflect off of the crystal, but it may also cause fluorescence, meaning the crystals themselves are a source of secondary X-rays. This is dependent upon the composition of the sample, if the sample contains elements that emit X-rays that are exciters of elements present in the crystal, the resultant fluorescence is extremely high. This can be mitigated through measuring the background radiation and then subtracting it from the intensity measured in the detector. (Willis and Duncan, 2008)

The collimator prevents unwanted secondary X-rays from reaching the detector, thereby improving the resolution of the device (Potts, 2005). To cover the wide range of X-ray wavelengths, WDXRF devices require multiple types of detectors. The two main types of detectors are:

- Scintillation counter - for short wavelengths,
- Gas flow proportional counter - for medium to long wavelengths. (Tuisku, 2018)

1.8 Sulphur and oil shale

Sulphur is a chemical element with the atomic number of 16 and the symbol of S. It is nonmetallic and relatively abundant, though it usually occurs as an ion within a mineral containing other chemical elements. It is an essential component for life, but sulphur and its compounds are major air pollutants, and have adverse effects on human health, such as bronchitis, bronchoconstriction and pulmonary resistance. The increasing prevalence of fuel refinement and smelting of sulphur compounds has led to a massive imbalance in the amount of sulphur in the environment. (Komarnisky et al, 2003)

Sulphur is present in multiple other fossil fuels including crude oil and natural gas in the form of compounds such as hydrogen sulphide (H_2S) or Sulphic dioxide (SO_2) (Raj et al, 2020). Oil shale remains of interest due to its abundance as a source of samples, through itself, its derivatives and detritus. While the exact properties of oil shale are dependent on its geographical origin, the sulphur content of Estonian oil shale is approximately 1-2 percent. (Maaten et al, 2018)

The K_α energy of sulphur is approximately 2307 eV (Experimental K-alpha X ray energies, 2005), which corresponds to a wavelength of approximately 0.537 nm, according to equation

(1). As it is an element with a relatively small atomic number, its L-series lines are too faint to be detected with modern XRF analysers. (Schoonjans et al, 2011)

1.9 Fluorescence yield and the Auger effect

The intensity of fluorescence is not uniform for all elements, this variation is known as the fluorescence yield of a given element, usually denoted by the letter ω. Elements with a lower atomic number have a lower fluorescence yield, with a corresponding higher yield of electrons absorbing the fluorescence photons and, as a result, escaping the atom. Fluorescence yield can be defined as the intensity of the excited radiation divided by the exciting radiation, or the number of X-rays emitted from the element divided by the number of X-rays used to cause the fluorescence: (Hevesy and Lay, 1934)

$$\omega = \frac{\sum n_i}{N} \tag{7}$$

Where ω is the fluorescence yield, n_i is the number of excited photons for line i and N is the total number of photons used to induce fluorescence.

The cause for this variation of X-ray output between different elements is the Auger effect. While an electron that has been excited by an incident photon of sufficient energy emits a fluorescence photon, that photon is not necessarily guaranteed to exit the electron shells. It is entirely possible for the resulting photon to be absorbed by another electron of the same atom (Hubbell, 2003). For elements with a low atomic number, the affected electron is likely a loosely bound valence electron, which will be ejected. For this reason, lighter elements have a lower fluorescence yield: their outer electrons are less strongly bound than those of heavier elements, making electron ejection and the prevention of an X-ray escaping more likely.

1.10 Uncertainty

To establish the reliability of repeated testing of data, it is necessary to gauge the uncertainty of the repeated measurements, which is known as type-A uncertainty. For this, a measure of average dispersion in relation to the mean value, known as the standard deviation, is required. This value is the square root of variance, the mean of the squared deviations of the data points from their mean.

$$s = \sqrt{\frac{\sum (x_i - \mu)^2}{n}} \tag{8}$$

where x_i is the individual value of a set at index i, μ is the mean value of the set, and n is the total amount of measurements.
The type-A uncertainty of a set of measurements can be found by dividing the standard deviation s of a series of data points by the square root of the total amount of measurements made n. (Dorozhovets, 2020)

$$U_A = \frac{s}{\sqrt{n}} \tag{9}$$

2 Methodology development for sulphur detection in oil shale using X-ray fluorescence spectrometry

2.1 Main devices

The main devices used for this thesis were the Rigaku ZSX Primus II and the Bruker S4 Pioneer, both of which are wavelength dispersive XRF devices. In terms of function, there is very little difference between the two devices, both are considered to produce identical analysis results. Where the devices diverge are the assumed size of the samples and the analysis process.

Figure 6. The Rigaku ZSX Primus II.

Figure 7. The Bruker S4 Pioneer.

Both devices utilize multiple receptacles to hold samples in place while they are analysed, with each individual sample being analysed sequentially. The Rigaku Primus utilized receptacles designed for solid (e.g. non-powder or liquid) samples with diameters of 32 millimetres, while the Bruker Pioneer utilized receptacles for diameters of 36 millimetres. The two devices could use samples interchangeably, but would require modifications to the sample cup, a smaller mask for the Bruker Pioneer for example.

Concerning the analysis process, the Rigaku Primus places the sample undergoing analysis into a separate chamber, where X-rays are directed through an opening on the top of the sample receptacle. The Bruker Pioneer is similar, using a separate chamber for analysis, but X-rays are directed through a slot in the bottom of the receptacle.

Given these differences between the two main devices utilized in this thesis, one point of interest during statistical analysis is whether divergences in machine function could lead to different analysis results.

2.2 Development process

The method development process can be divided into three parts: preparation of samples, pre-optimization of the measuring parameters for the case of sulphur measurement, and quantitative analysis of the measuring results. The former two are the two parameters that were sought to optimize further to develop the measuring methods, and the final one was a source of data to achieve this.

Sample preparation did not require optimization, as comparing results between different types of samples was one of the goals of the thesis. The only conditions pertaining to samples to affect the choice of sample type were the availability of different reagent materials and the probability of the preparation to produce any acceptable results at all. The points of interest for analysis were: time and energy required for the sample creation process, amount of material (both sample and binder/dilutant) and variability of results within the same sample creation method.

Pre-optimization was conducted based on previously established theoretical information. There was only one element of interest, sulphur, and all relevant and feasibly modifiable parameters were changed to increase detection sensitivity and spectrum accuracy for this element.

Post-measurement results were the sole source of information as to how both sample preparation and changing measurement parameters can be developed to be further optimized for sulphur detection.

2.3 Preparation of samples

Proper preparation of samples is key to achieving clear XRF spectra that are fit for analysis. The solid non-powder samples were glass discs of relatively small size, for the particular machines used in this thesis, they had to be approximately 32-36 millimetres in diameter and 4-8 millimetres in thickness. All different forms were considered to ascertain the suitability of each for detecting sulphur.

2.3.1 Basic principle

Regardless of the particulars of the sample's consistency, a few basic criteria for samples were observed. These are:

- The sample must be representative of the material being researched as a whole,
- the sample must be homogeneous, as only the surface layer can be analysed,
- the sample cannot be contaminated.

The samples were placed in a sample cup, with a transparent supporting film used for methods that could potentially loose particles into the surrounding environment, such as loose powder. These receptacles were then placed into the XRF analyser, where they were sequentially analysed.

2.3.2 Solid

Completely solid homogeneous samples require a minimum of preparation, with only some removal of surface dust necessary to decontaminate and initiate analysis. The only issue with them is the shape, if the samples do not fit in the receptacles, they must be reduced in size. This presents the danger of being turned into a size unfit for analysis, if the sample is too small, the X-rays may instead excite the receptacle they are placed in, causing the spectrum to become inaccurate. Because of this, and to avoid possible inhomogeneous samples, it was decided to instead turn solid samples into a powder.

2.3.3 Powder

A problem presents itself when a solid sample material is not already homogeneous, as there are no ways to keep a solid in its original shape while changing its internal construction. For this reason, the only way to homogenize the sample would be to pulverize it into a fine powder. This issue proved to be simple to solve, as the sample material was relatively brittle oil shale, while other samples were already in the form of a fine powder, such as oil shale ash. Without any additional preparation, powder samples only require careful placement into the receptacle and a cover of protective film to prevent loose particles from being released into the measuring environment.

However, as this caused a variety of issues including raising the amount of time necessary for re-analysis and potentially still causing loose particles to be scattered into the testing environment, the amount of loose powder samples was kept to a minimum, only 3 samples.

While some sample materials already exist in the form of a powder, there still exist irregularities in their composition, such as clumps. These irregularities may lead to inhomogeneities and inaccurate analysis results. To prevent this, all samples derived from powders were pulverised with either a mortar and pestle or an automated planetary ball mill, the Retsch PM 100. It was presumed that manually processed samples would have more inaccurate results than those that were pulverised using the automatic mill.

2.3.4 Press pellet

An alternative to directly analysing a powdered sample would be to subject it to high pressure (200 kN) to produce a hardened pellet that does not require a covering of protective film. While this means that there is no need to apply protective films to sample receptacles, the

process of creating pellets is a time-consuming process. However, once created, the pellets can easily be analysed in multiple different analysis sessions, assuming that the sample has been handled properly and has not become contaminated.

For this purpose the pellet press Atlas Autotouch XRF was used to produce sample pellets, which made up the majority of samples used for creation of X-ray spectra. While the maximum pressing force of the machine is 40 tons, regular samples are usually pressed with a force of only 18 tons. As this still caused samples to fracture, the pressure was subsequently increased to 21 tons.

Initially, a mass of 5 grams was chosen with a 4 to 1 ratio of sample material and binder, meaning 4 grams of reagent and 1 gram of binding agent. The binder used was micropowder C ($C_{38}H_{76}N_2O_2$), manufactured by the LGC standards. It is a Hoechst wax based binder, and while it does theoretically affect the chemical composition of the sample, this is accounted for during calibration and does not noticeably change the detected concentration of sulphur within the sample material. In a trial run of 10 pellets, this resulted in solid and efficiently analysable samples, but 50% of pellets pressed of such a mass were brittle and crumbled either immediately or upon light handling. To alleviate this issue, the mass of each pellet was doubled to 10 grams while preserving the ratio of reagent and binder. This means 8 grams of sample material and 2 grams of binder, which resulted in more resilient samples, only 5% of samples fractured due to innate brittleness of the sample. This increased mass also reduced the chance of destruction from errors during handling.

Both analysers accept a sample diameter size of 32 millimetres, but only one of them accepts up to 36 millimetres. While 32 millimetre diameter samples made up the majority of samples analysed, a few larger samples were also created to see if there is a difference in resolution or accuracy.

Figure 8. Example of a pressed sample pellet with a diameter of 32 millimetres.

In total, 32 pellet samples were created, 10 with a diameter of 32 millimetres and 22 with a diameter of 36 millimetres.

2.3.5 Beads

Another possibility for simplifying powder sample analysis would be to melt it with a binding additive at a high temperature, 900-1200 degrees Celsius, to produce a homogeneous glass bead. As with press pellets, adding a binding agent alters the composition of the sample, but melting samples also causes evaporation of water, carbon dioxide and other elements, further changing the chemical makeup of the sample. As sulphur is also a candidate for leaving the sample during the melting process, bead samples as seen on figure 9 were used for analysis, to gauge the effect of heating on analysis results.

Figure 9. Example of a bead sample with a diameter of 36 millimetres.

The benefits and drawbacks of this method are very similar to that of the pellet method, but far more intense. The amount of time and energy needed to produce one bead is even greater than that needed for pellet creation, but beads are even more resistant towards contamination and can produce clearer results.

The production of beads was achieved with an automated fusion fluxer. Similarly to the pellet method, a binding agent must be added to the reagent material to create a suitable sample. In this case, the binding agent used was a mix of lithium tetraborate, lithium metaborate and lithium borate, with concentrations of 49.75%, 49.75% and 0.50 % respectively. The ratio of reagent to binder was 1 to 10, 1 gram of reagent and 10 grams of binder to produce a single fused bead sample.

The evaporation of material from the sample during the melting process is observable through a change in mass, which is called the loss on ignition, henceforth referred to as the LOI. The estimated LOI was observed and calculated for all samples, with the average of all sample LOIs being considered for analysis of results.

A total of 15 beads were created by melting at a temperature of 950 °C and analysed.

2.3.6 Liquid

Liquid samples require similar preparation to powder, as it is also a type of sample that is in danger of spreading loose particles into its surroundings. Most liquid samples are also already homogenized, but may require diluents to obtain sufficient liquid. In addition, liquid samples cannot be analysed in a vacuum, as the liquid would evaporate. The analysing chamber must be filled with helium, as it serves to keep the liquid within its receptacle while minimizing absorption of X-rays by the surrounding environment. For this reason, liquid samples were not analysed, as the only XRF analysis machine used did not have a sufficient supply of helium to conduct an analysis of acceptable quality.

2.4 Sample reagents

The material for the samples was oil shale ash, extracted from boiler 8 of the Auvere electricity plant in Ida-Virumaa, Estonia. As oil shale is a fossil fuel extensively mined and utilized in Estonia, its relative abundance as a source of sample material was evident. The existence of sulphur within oil shale is well established, determining its existence and concentration from fuel use residue is presumably very simple. Additionally, as oil shale ash is already a fine powder, it would minimize the amount of necessary pre-analysis sample preparation.

A total of approximately 500 grams of sample material was utilized to create all of the samples analysed in this thesis.

2.5 Optimization

Before proper quantitative analysis may begin, the measuring conditions of the samples must be optimized according to previously present theoretical data.

The first parameter that had to be considered was the anode for the X-ray tube utilized in the XRF analysis instrument. While it is true that any anode that releases photons of high enough energy would be sufficient, the spectrum emitted by the target material is still a spectrum, and may overlap with the element being analysed. This is problematic, as it means that the output series lines may not actually be caused by any sulphur contained within the sample, but by the anode itself. To prevent this, a complementary anode should be chosen, silver (Ag) to be precise, but this was not possible due to a lack of access to an anode of said material and the amount of time and effort necessary for exchanging anodes within the machines. Additionally, while such a change would optimize the machines for sulphur, other elements were still considered insofar as how difficult it would be to return a machine from sulphur optimization to a state suitable for general analysis. Changing the anode is time consuming, and for users who wish to analyse a more general spectrum of elements, it would be unthinkable to swap anodes purely for sulphur.

The second parameter is the calibration through analysis of a calibration sample. This does not require exchanging hardware within the machine itself, only analysing the calibration standard as a normal sample, then compiling the results into a calibration curve, a graph that plots the intensity of a detected peak to the concentration of the element within the calibration standard.

2.6 Quantitative analysis

After multiple sets of analyses for both powder pellets and fused beads, the results were tabulated and analysed using Microsoft Excel. All concentrations were measured to a third decimal place, and all values calculated from them were rounded to a second decimal place. The main measured element was sulphur trioxide, the main sulphur component within the reagent.

Measurement results were compared based on two criteria: machine used and size of sample where applicable. Additionally, results were compared between the two different types of sample preparation, pressed pellets and fused beads.

2.6.1 Results, pressed pellets

Two sets of pressed pellets, 32 millimetre and 36 millimetre diameter samples, were analysed in both devices. Firstly, the difference of results between the two WDXRF machines was examined.

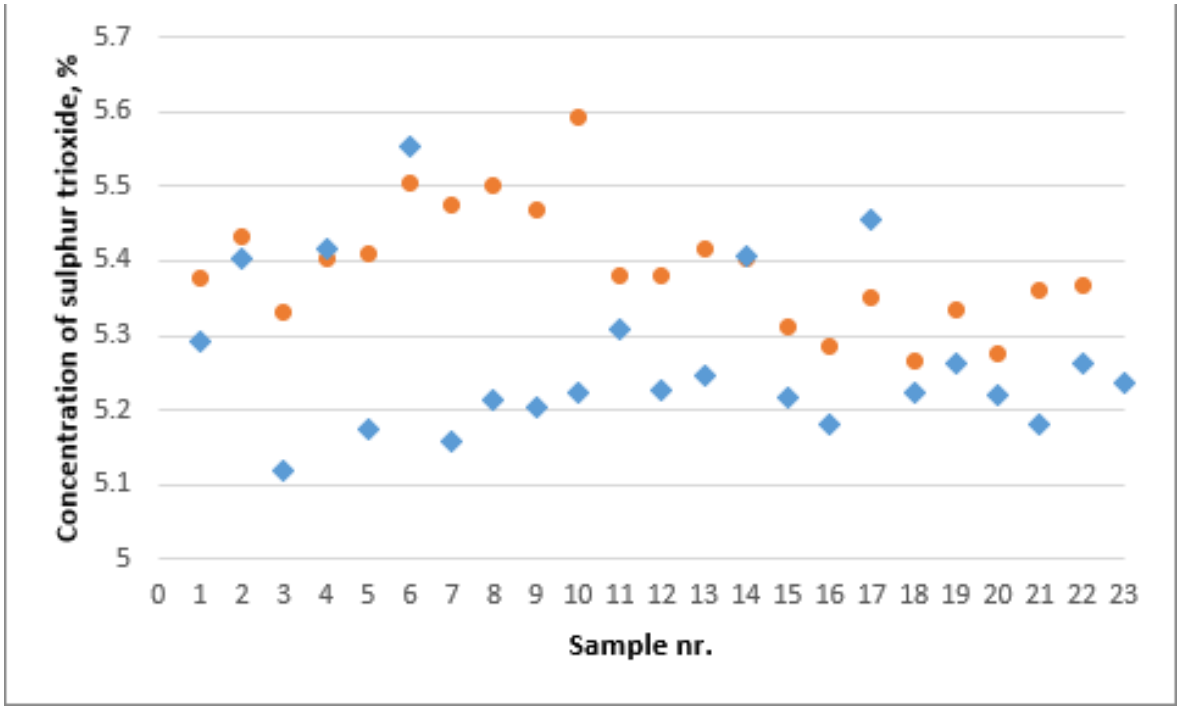

Figure 10. Results of 36 millimetre diameter pressed pellet sample analysis on two different WDXRF machines. The blue and orange dots represent the results of the Rigaku and Bruker, respectively.

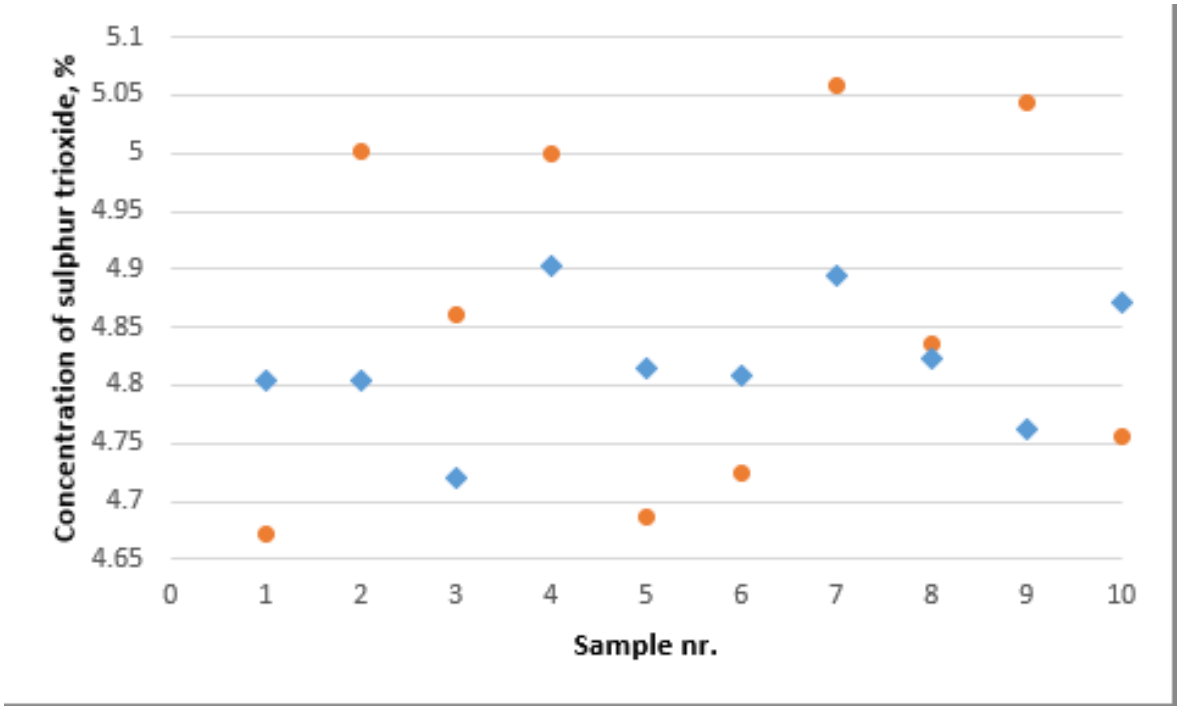

Figure 11. Results of 32 millimetre diameter pressed pellet sample analysis on two different WDXRF machines. The blue and orange dots represent the results of the Rigaku and Bruker, respectively.

The 36 millimetre samples saw a slight divergence as the average concentration value between the analysis sets was 0.12%. The 32 millimetre samples showed hardly any differences at all,

with average concentration values being different by only 0.04%, a relative difference of 0.83%.

Secondly, samples of different sizes were compared.

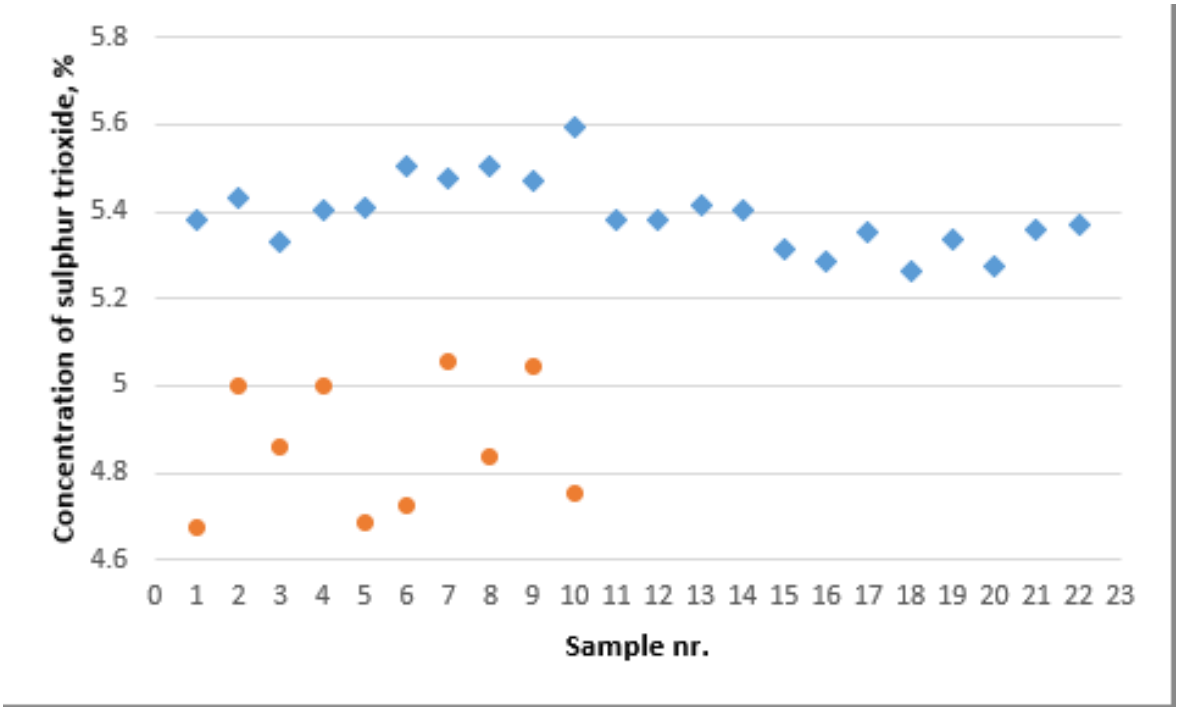

Figure 12. Results of two different sample diameters. The blue and orange dots represent the concentrations of 36 millimetre and 32 millimetre diameter samples, respectively.

There is an explicit distinction between the two sample diameter sizes, 32 millimetre samples have an average value 0.53% concentration percent below that of the 36 millimetre sample average value, corresponding to a relative difference of 10.91%. To establish whether this is a measurement error or not, the 32 millimetre samples were measured again and compared to the original results.

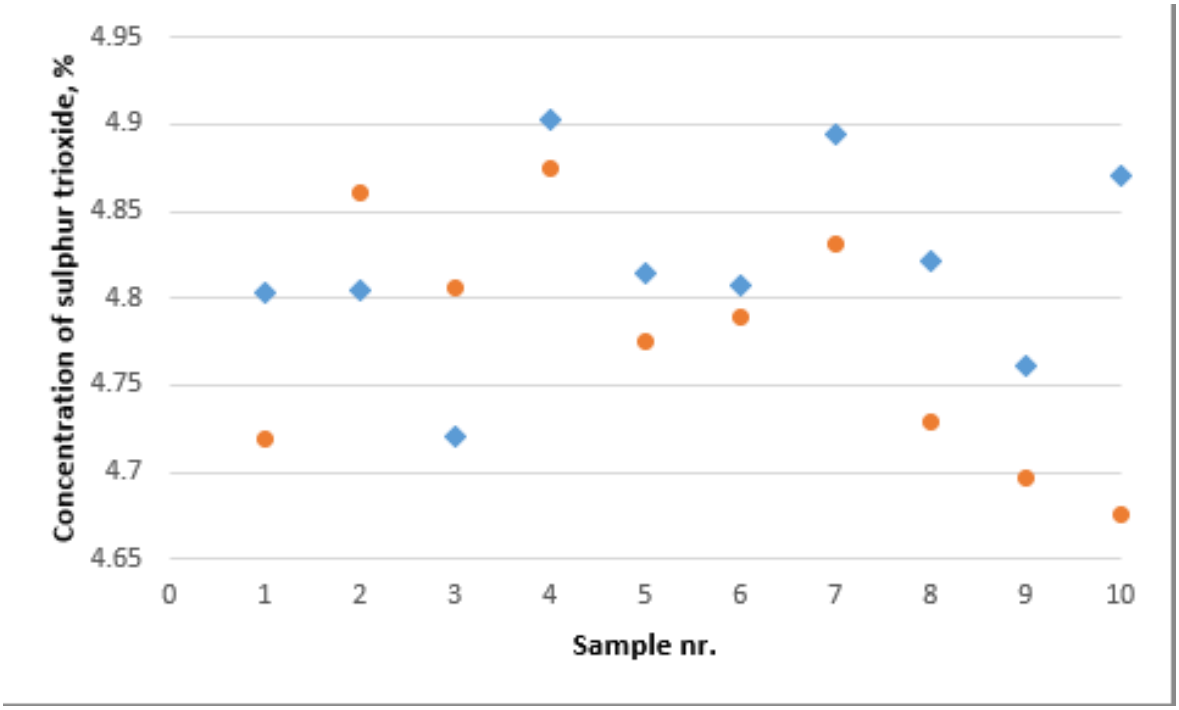

Figure 13. Results of repeat measurements of 32 millimetre pressed pellets. The blue and orange dots represent the first and second set of measurements, respectively.

The measurements of 32 millimetre samples did not reveal any noticeable discrepancies due to repeated analysis, a difference of 0.04% between average values of test series.

The standard deviation was calculated using equation (9), and was 0.14 for 32 millimetre samples, and 0.08 grams for 36 millimetre samples. The type-A uncertainty of the pressed pellet measurements was 0.05 grams for 32 millimetre samples, and 0.02 grams for 36 millimetre samples.

2.6.2 Results, beads

The average LOI was calculated to be 11.19%.

To establish there is a difference of results between measuring instruments, the same 15 fused bead samples were analysed by both machines and the values were compared.

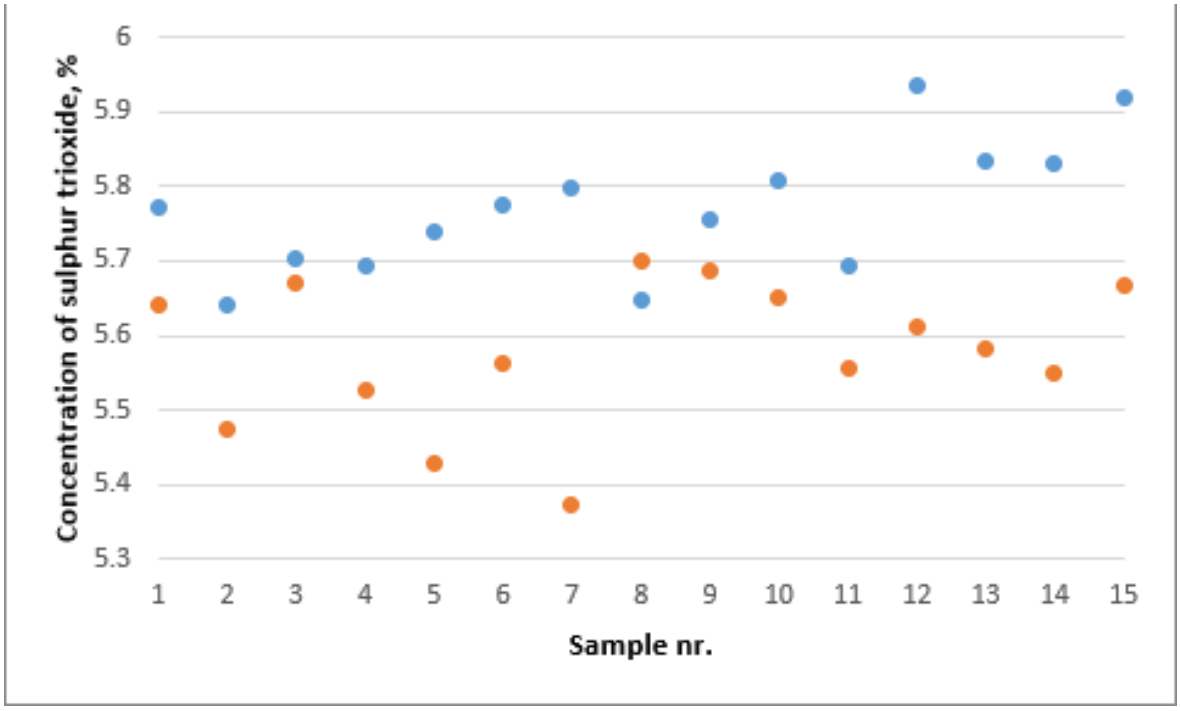

Figure 14. Results of fused bead sample analysis on two different WDXRF machines. The blue and orange dots represent the results of the Bruker and Rigaku, respectively.

The Rigaku repeatedly detected lower amounts of sulphur than the Bruker. The difference between the average values of sulphur differed by 0.19% of concentration, a relative difference of 3.4%. This falls below the generally accepted error margin of 5%, but the consistent difference in results was still noteworthy.

To estimate the reliability of fused bead analyses, the measurements were repeated for the entire set of samples, following the same procedure as during the first measurement: results were tabulated, the average concentration of all detected elements were calculated, and then absolute and relative standard deviations were established. The concentrations of sulphur trioxide were compared to the results of the previous set of measurements with the same machine to estimate the extent to which measuring errors cause a variance in analysis results.

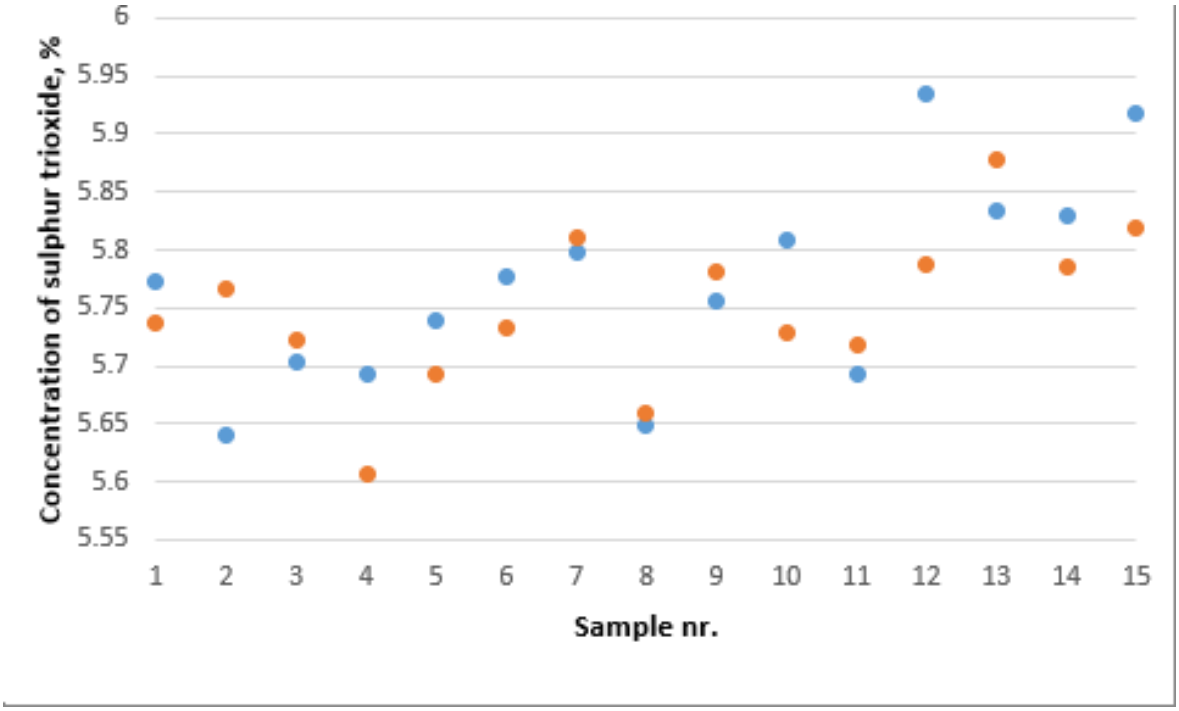

Figure 15. Results of repeated testing of fused bead samples. The blue and orange dots represent the results of the first and second set of measurements, respectively.

The variance created by repeated measurement was minimal, four samples produced nearly identical results (relative difference of values below 0.50%) both times. The greatest relative difference in values was with sample number 12, 2.54%.

Once again, the type-A uncertainties were calculated. The standard deviation of fused beads was 0.08 grams, with an uncertainty of 0.02 grams.

2.6.3 Pressed pellets versus fused beads

By examining the results of both the pressed pellet and fused bead test series, their merits relative to each other could be determined.

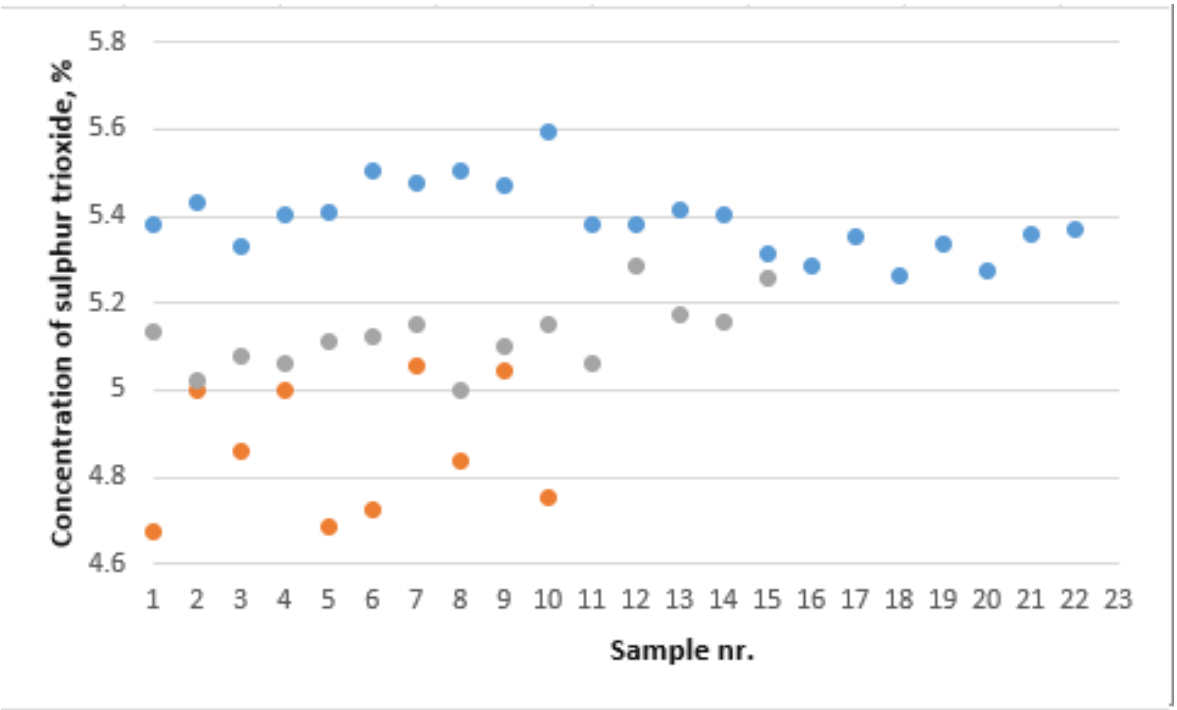

Figure 16. Results of pressed pellet versus fused bead analysis. The blue, grey and orange dots represent the results of the fused bead, 36 millimetre pellet and 32 millimetre pellet measurements, respectively.

It is clear that there is a large difference between pellets and beads, as can be seen from the difference between the arithmetic averages of each set of measurements: 5.12 grams for glass beads, 5.39 grams for 36 millimetre pellets and 4.86 grams for 32 millimetre pellets. As these differences are much greater than the uncertainties of any of the analysis sets, it could be inferred that this is not a result of random chance.

The true reasons for these differences are less clear. It could be that introducing the sample material to high temperatures and thereby causing a loss of mass in the sample also causes the proportion of sulphur to rise. The addition of a binding agent would also cause a change in mass, but the complex molecules introduced by binders cannot be detected as molecules, only as the elements within them. Neither of the binders used contained sulphur, meaning they cannot cause interference during analysis.

Of note is also the contrast between the results of the pellets of different diameters. The 32 millimetre samples show great volatility in their testing results, but still remain firmly beneath the set of 36 millimetre samples.

3 Summary

A total of 71 measurements were made with pressed pellets and fused beads.

It is clear that the effect that a difference in measuring device results in negligible deviances in sulphur content concentrations, easily explained by measuring uncertainty. Likewise, repeated measurements for both types of samples had minimal discrepancies, they can be considered to be equally repeatable, mechanical fragility aside.

Comparing measurements of pellets or beads reveals that differing sample types do result in a difference in measured sulphur concentrations. This can be somewhat explained by the loss on ignition of the beads evaporating certain amounts of sulphur before measurement. Furthermore, the pellets with non-identical dimensions also returned noticeable discrepancies between sulphur content levels. This may have been caused due to differences involved in the preparation of samples. Regardless, the differences can be considered to be minor.

Both varieties of sample can be considered reliable methods for sulphur measurement, but pressed pellets require less time for a greater amount of samples. This can be important for creating large sets of measurements.

Overall, the results revealed much about the nature of different types of sample preparation and X-ray fluorescence spectrometry involving sulphur, as well as opening new avenues for further optimization of sulphur detection.

4 Acknowledgements

The author of this thesis would like to extend heartfelt and sincere thanks to Nata-Ly Pantšenko, Alar Konist, Jaan Kalda and Toivo Kallaste.

5 Reference material

1. International Energy Agency. (2013). Energy Policies Beyond IEA Countries: Estonia 2013. https://doi.org/10.1787/9789264190801-en

2. Brouwer, P. (2013). Theory of XRF : getting acquainted with the principles. PANalytical B.V.

3. Tugulan, L. C. Duliu, O. G. Gradinaru, J. (2016). An EDXRF and WDXRF intercomparison case study: Major elements content of dobrogea loess. Romanian Journal of Physics Vol. 61(Nos. 9-10) 1626-1634

4. Murphy, A. Sciacca, F. Bell, D. et al. (2017). Photon. https://radiopaedia.org/articles/52703 Retrieved: 12.03.2023

5. Willis, J. P. Duncan, A. R. (2008). Understanding XRF spectrometry. PANalytical B.V.

6. Fewster, P. F. (2015). X-ray Scattering From Semiconductors And Other Materials (3rd Edition). World Scientific.

7. Fernandez, J. E. (1992). Rayleigh and Compton scattering contributions to x-ray fluorescence intensity. https://doi.org/10.1002/xrs.1300210204

8. Turchetta, R. (2014). Complementary metal-oxide semiconductor (CMOS) sensors for high-performance scientific imaging. In: Durini, D (Ed.), High Performance Silicon Imaging (pp. 281-311). Woodhead Publishing. https://doi.org/10.1533/9780857097521.2.281.

9. Hamouda, S. (2020). Compton Scattering: A Theory and Experiments. https://www.researchgate.net/publication/343691574_ Compton_ Scattering_ A_ Theory_ and_ Experiments

10. Rojo, A. G. Berman, P. R. (2010). Rayleigh scattering revisited. In: American Journal of Physics. (pp. 94-101) https://doi.org/10.1119/1.3236688

11. Baird, C. S. (2019). Absorption of electromagnetic radiation. AccessScience. https://doi.org/10.1036/1
8542.001600. Retrieved: 21.04.2023.

12. Hussein, E. M. A. (2007). Radiation Mechanics. Elsevier Science Ltd. https://doi.org/10.1016/B978-008045053-7/50002-1.

13. University of Central Florida. (2016). The Photoelectric Effect. https://pressbooks.online.ucf.edu/phy2053bc/chapter/the-photoelectric-effect/ Retrieved: 17.04.2023.

14. Schäfers, K. P. Bolwin, K. Büther, F. Hermann, S. Jacobs, A. H. Kösters, T. Kuhlmann, M. Schäfers, M. Viel, T. (2014). 1.10 - High-Resolution Small Animal Imaging. In: Brahme, A. (Ed.), Comprehensive Biomedical Physics. Elsevier. (pp. 181-211) https://doi.org/10.1016
0-444-53632-7.00110-6.

15. Kang, I-J. Foland, W. D. (1967). Theory of Electron Impact Excitation and Ionization of Atoms and Ions. In: Phys. Rev. Vol. 164 Issue 1. American Physical Society. (pp. 122-130). DOI: 10.1103/PhysRev.164.122

16. Etim, I. Rebecca, M. (2022). A comparison of the performance and energy resolution of CdTe and Si detectors in the X-ray Fluorescence studies of metal samples and Alloys. In: Journal of the Nigerian Society of Physical Sciences. DOI:10.46481/jnsps.2022.926

17. Jenkins, R. Manne, R. Robin, R. Senemaud, C. (1991). Nomenclature system for X-ray spectroscopy. In: Pure & Appl. Chem. IUPAC. Vol 63. No 5. (pp. 735-746)

18. L'Annuziata, M. F. (2003). Nuclear radiation, its interaction with matter and radioisotope decay. In: Handbook of Radioactivity Analysis (Second Edition). Academic Press. (pp. 1-121). https://doi.org/10.1016/B978-012436603-9/50006-5.

19. Laguitton, D. Parrish, W. (1977). Experimental Spectral Distribution versus Kramers' Law for Quantitative X-ray Fluorescence by the Fundamental Parameters Method. In: X-ray Spectrometry Vol 6 Issue 4. (pp. 201) https://doi.org/10.1002/xrs.1300060409

20. Guthrie, J. M. Ferguson, J. R. (2012). XRF Technical Overview. https://archaeometry.missouri.edu/xrf_ technical.html Retrieved: 23.07.2023.

21. Darwell, B. W. (2018). Chapter 26 - Radiography. In: Materials Science for Dentistry (Tenth Edition). Woodhead Publishing. (pp. 665-698) https://doi.org/10.1016/B978-0-08-101035-8.50026-2.

22. Kramar, U. (1999). X-Ray Fluorescence Spectrometers. In: Lindon, J. C. (Ed.), Encyclopedia of Spectroscopy and Spectrometry (Second Edition), Academic Press. (pp. 2989-2999) https://doi.org/10.1016/B978-0-12-374413-5.00314-6.

23. Potts, P. J. (2005). X-RAY FLUORESCENCE AND EMISSION | Wavelength Dispersive X-Ray Fluorescence. In: Worsfold, P. Townshend, A. Poole, C. (Ed.), Encyclopedia of Analytical Science (Second Edition). Elsevier. (pp. 419-429) https://doi.org/10.1016/B0-12-369397-7/00674-9.

24. Tuisku, A. (2018). Wavelength Dispersive X-ray Fluorescence Method Development for Asphaltene Samples. Metropolia University of Applied Sciences.

25. Gonzalez, A. (2012). X-ray Crystallography: Data Collection Strategies and Resources. In: Egelman, E. H. (Ed.), Comprehensive Biophysics. Elsevier. (pp. 64-91) https://doi.org/10.1016/B978-0-12-374920-8.00106-5.

26. White, S. C. Pharoah, M. J. (2014). Chapter 1 - Physics. In: Oral Radiology (Seventh Edition), Mosby. (pp. 1-15) https://doi.org/10.1016/B978-0-323-09633-1.00001-8.

27. Komarnisky, L. A. Christopherson, R. J. Basu, T. K. (2003). Sulfur: its clinical and toxicologic aspects. Nutrition. doi: 10.1016/s0899-9007(02)00833-x.

28. Raj, A. Ibrahim, S. Jagannath, A. (2020). Combustion kinetics of H2S and other sulfurous species with relevance to industrial processes. In: Progress in Energy and Combustion Science, Vol 80. https://doi.org/10.1016/j.pecs.2020.100848.

29. Maaten, B. Pikkor, H. Konist, A. Siirde, A. (2018). Determination of the Total Sulphur Content of Oil Shale Using Different Analytical Methods. In: Oil Shale Vol. 35, No. 2. (pp. 144-153) https//doi.org/10.3176/oil.2018.2.04

30. Schoonjans, T. Brunetti, A. Golosio, B. del Rio, M. S. Sole, V. A. Ferrero, C. Vincze, L. (2011). The xraylib library for X-ray–matter interactions. Recent developments. In: Spectrochimica Acta Part B: Atomic Spectroscopy Vol. 66, No. 11-12. (pp. 776-784) https://doi.org/10.1016/j.sab.2011.09.011.

31. Georgia State University (2005). Experimental K-alpha x ray energies. http://hyperphysics.phy-astr.gsu.edu/hbase/Tables/kxray.html Retrieved: 06.08.2023

32. Hevesy, G. Lay, H. (1934). Fluorescent Yield of X-ray Emission. In: Nature, Vol 134. (pp. 98-99) https://doi.org/10.1038/134098b0

33. Hubbell, J. H. (2003). Radiation Physics. In: Meyers, R. A. (Ed.), Encyclopedia of Physical Science and Technology (Third Edition). Academic Press. (pp. 561-580). https://doi.org/10.1016/B0-12-227410-5/00634-7.

34. Dorozhovets, M. (2020). Forward and inverse problems of Type A uncertainty evaluation. In: Measurement, Vol 165. https://doi.org/10.1016/j.measurement.2020.108072.